Non-stoichiometric crystal nucleation in a spodumene glass containing TiO_2 as seed former: effects on the viscosity of the residual melt

Alessio Zandonà[1,2,*], Alex Scarani[3], Jessica Löschmann[4], Maria Rita Cicconi[2], Fabrizio Di Fiore[3], Dominique de Ligny[2], Joachim Deubener[4], Alessandro Vona[3], Mathieu Allix[1], Danilo Di Genova[5]

[1] CNRS, CEMHTI UPR3079, Univ. Orléans, F-45071 Orléans, France

[2] Friedrich-Alexander-Universität Erlangen-Nürnberg, Department of Materials Science (Glass and Ceramics), Martensstr. 5, 91058 Erlangen, Germany

[3] Dipartimento di Scienze, Università degli Studi Roma Tre, Largo San L. Murialdo 1, 00146 Rome, Italy

[4] Institute of Non-metallic Materials, Clausthal University of Technology, Zehntnerstraße 2a, D-38678 Clausthal-Zellerfeld, Germany

[5] Institute of Environmental Geology and Geoengineering (IGAG), CNR, via Salaria km 29.300, 00015 Monterotondo, Rome, Italy

Abstract

A spodumene glass ($LiAlSi_2O_6$), doped with 4 mol% TiO_2 as nucleating agent, was synthesized by containerless melting. Its accurate viscosity characterization by micropenetration viscometry or calorimetry is shown to be very challenging in the vicinity of the glass transition, due to the unpreventable occurrence of thermally activated non-stoichiometric crystal nucleation, closely overlapping the relaxation into the liquid state. TiO_2 crystal nucleation brings about a compositional modification of the residual melt, with an associated increase in measured viscosity by up to 2 log units. A careful experimental approach and a profound understanding of seed formation are essential to circumvent or at least minimize such inaccuracies, getting as close as possible to the viscosity of the parent homogeneous melt.

Keywords: glass transition temperature; parent melt; non-stoichiometric crystallization; glass-ceramics containing seed formers; TiO_2.

***Corresponding author:** Alessio Zandonà, alessio.zandona@fau.de

1. Introduction

Glasses play an essential role in a wide range of technological applications, from telecommunications relying on low-loss optical fibers to regenerative medicine based on 45S5 bioactive glass [1]. Moreover, they act as precursors for the synthesis of glass-ceramics, obtained by controlled crystallization [2] and exhibiting unique advantageous properties such as zero thermal expansion, transparency, extremely high toughness and/or good machinability depending on the chosen compositional systems [3,4]. Irrespectively of the selected application, a precise knowledge of the temperature-dependent viscosity η(T) of glass-forming melts is key to achieve successful homogenization, fining and shaping of the final product [5,6]. Furthermore, viscosity must be carefully controlled during crystallization heat treatments, to harness crystal growth kinetics [7] and avoid undesired deformation and cracking during the production of glass-ceramics [4].

Viscosity η(T) is best described using three-parameter non-linear equations, such as the Vogel-Fulcher-Tammann (VFT) [8–10], the Adam-Gibbs (AG) [11] or the Mauro-Yue-Ellison-Gupta-Allan (MYEGA) [12] formulations, which are fitted to experimental data typically obtained above the liquidus temperature T_m (e.g., by concentric-cylinder rheometry) and in the vicinity of the glass transition temperature T_g where $\eta = 10^{12}$ Pa s (e.g., by micropenetration viscometry, beam-bending viscometry or calorimetry). However, experiments performed at subliquidus conditions can prove rather challenging in melts with a limited glass-forming ability

(and glasses with poor glass stability [13]), as phase separation and crystallization may occur, hampering reliable determination of the viscosity of the homogeneous parent liquid.

Several authors examined the effects of partial crystallization on viscosity: apart from the long-known increase in effective viscosity due to the presence of suspended solid particles [14], the non-stoichiometric precipitation of crystal phases was recently shown to possibly reduce [15] or augment [16,17] the local viscosity of the residual melt by several orders of magnitude, due to the preferential extraction of certain chemical components. Moreover, nanoscale heterogeneities produced by diffusion before and during crystal nucleation (e.g., compositional enrichments or shells around crystals [18–20]) were suggested to increase significantly the effective viscosity of the system, far beyond the mere chemical modification of the carrier liquid phase [21]. Such observations have far-reaching implications also in the field of volcanology, since non-stoichiometric (nano)crystallization due to silicate melt supercooling and transition metal supersaturation has been recently suggested to crucially trigger explosive episodes during effusive eruptions, due to viscosity increase and simultaneous promotion of bubble nucleation [21–26].

In this work, we exemplify how the correct experimental determination of the viscosity of homogeneous parent melts is arduous and virtually unachievable for glasses supersaturated in transition metal oxides [27,28], e.g., aluminosilicate liquids containing TiO_2 or ZrO_2 as nucleating agents (also recalled as seed formers in the following). Non-stoichiometric phase separation and/or nanocrystallization take place in these materials as soon as T_g is approached, in a close interplay with structural relaxation processes. Though involving only a few mol% of nucleating agents, non-stoichiometric crystal nucleation can notably lead to a rise in the viscosity of the residual melt (whose chemical composition evolves during the actual measurements) by one log unit or more [21], possibly leading to substantial experimental errors. Though operatively unavoidable even using state-of-the-art instrumentation, such inaccuracies

can be minimized with a suitable experimental approach (as recently illustrated for volcanic melts [23]), getting as close as possible to the crystal-free parent melt viscosity.

2. Experimental

2.1. Glass synthesis

Lithium aluminosilicate (LAS) glass of spodumene stoichiometry ($LiAlSi_2O_6$), doped with 4 mol% TiO_2, was chosen for the investigations since the crystallization sequence of this material was previously shown to effectively schematize the thermal behaviour of zero-thermal-expansion LAS glass-ceramics during heat treatments [29,30]. The glass was synthesized by aerodynamic levitation coupled to laser heating (ADL) as described elsewhere [27,28,31]: Li_2CO_3 (99%, Aldrich), Al_2O_3 (99.999%, Strem Chemicals), SiO_2 (99.999%, Strem Chemicals) and TiO_2 (99.5%, Evonik P25) powder precursors were thoroughly mixed in an agate mortar and then pressed into pellets of approximately 1 g. Using the ADL device available at CNRS CEMHTI in Orléans (France), small chunks of these pellets were levitated in an O_2 flow, melted in containerless conditions at ~1700 °C for 5 s and quenched into glasses. As demonstrated in recent publications, these melting conditions enable reliable ADL synthesis of lithium (alumino)silicate glasses without evaporation losses, due to the comparatively low volatility of lithium with respect to other alkalis [27,32]. Each of the obtained glass beads had a diameter of ~2 mm and weighed 20–30 mg.

2.2. (Flash) Differential Scanning Calorimetry

Shards of crushed glass beads (mass in the range 8–20 mg) were used for calorimetric measurements at TU Clausthal, which were performed using a differential scanning calorimeter (DSC, 404 F3 Pegasus, Netzsch), in lidded PtRh20 crucibles and under N_2 5.0 atmosphere (25-80 ml min^{-1} flow rate). To obtain an overview of the crystallization sequence, the starting glass was measured at 5 or 10 K min^{-1} up to 1200 °C.

Measurements in the glass transition interval were performed using the rate-matching method [21,33–37], which involves: (i) a first heating segment (in this work, most typically at 10 K min^{-1}), which is necessary to bring the glass sample into the liquid state (i.e. beyond the onset of its glass transition) and erase the previous cooling history; (ii) a cooling segment at a selected rate q_c (in this work, 5, 10 or 20 K min^{-1}) down to room temperature; (iii) the actual measurement, corresponding to a second heating segment with q_h=q_c. During this latter segment, the characteristic glass transition temperature T_{onset} can be identified as the intersection of tangents drawn in the flat portion preceding the glass transition and at the flex point of the DSC trace during the glass transition. To demonstrate the reproducibility of this geometrical construction, we acquired here single DSC upscans at 10 K min^{-1} from 20 distinct TiO_2-doped spodumene glass beads and estimated a maximum uncertainty of ±5 K (possibly arising also from minor compositional differences between the beads). A more accurate method involving the mathematical analysis of the 2nd derivative of the DSC signal was recently proposed [38], but it was not applied here due to its impractical implementation in the case of unstable glasses undergoing sample modification (e.g., phase separation and crystallization) already during the first DSC upscan.

Due to the application of the rate-matching method, the thermal history of the samples is well-defined and therefore a viscosity value can be associated with T_{onset} through the relationship (Eq. 1):

$$log_{10}\eta(T_{onset}) = K_{onset} - log_{10}(q_h) \qquad \text{(Eq. 1)}$$

where K_{onset} is a chemically invariant constant, calibrated to 11.2(2) log Pa s [21]. For q_c=q_h = 10 K min^{-1}, the equation yields $\eta(T_{onset})$ = $10^{11.98}$ ≈ 10^{12} Pa s, in accordance with the most widespread convention in glass science. In previous works [21,34], also other characteristic temperatures were taken into account (T_{peak} and T_{liquid}, i.e. the signal undershoot during the glass

transition and the offset of the glass transition): they are disregarded here since they were, completely or partially, overlapped by TiO_2-driven seed formation, making their determination unreliable. In the following, the samples are named according to the parameters used during DSC measurements by the rate-matching method, i.e. $q_c=q_h$ and the maximum temperature (T_{max}) reached during the measurements (T_{max}). For instance, a sample measured at 10 K min^{-1} up to a T_{max} of 705 °C is recalled as 10DSC705.

The viscosity of the starting (homogeneous and crystal-free) parent melt was investigated also by flash differential scanning calorimetry (FDSC), according to the experimental procedure optimized in previous studies [33,34,37,39,40]. The used instrument was a Flash DSC 2+ (Mettler-Toledo) equipped with a UFH 1 sensor (operating range: -95 and +1000 °C) under constant flow of Ar 5.0 (40 ml min^{-1}). Small glass fragments obtained after crushing an ADL bead were selected and loaded into the instrument. To create a minimum contact between the glass samples and the measuring chip, they were first heated to 900 °C at a rate q_h of 1000 K s^{-1} and held at this temperature for 0.1 s, before cooling them at the same rate. However, a non-negligible thermal lag and probably an incipient crystallization affected most of our results due to this procedure (the obtained T_{onset} values spread over 60 K); indeed, the high T_m of the samples (~1400 °C [30]) prevented their full remelting on the chip, which represents the optimal condition for sample contacting during FDSC [33,37]. The actual measurements consisted of an identical thermal cycle at 1000 K s^{-1}, during which the heat flow signal was recorded to determine T_{onset}. Since both thermal lag and crystallization are expected to shift T_{onset} to higher temperature, we considered the lowest obtained value as the most appropriate to derive an associated viscosity through Equation 1 (see the Discussion section). In all cases, a temperature correction was performed based on the melting point of metallic indium (429.8 K).

2.3. Viscometry

A glass bead was polished into a plane-parallel plate of thickness ~1.5 mm and used to perform a viscosity measurement in the vicinity of T_g by the micropenetration method. The vertical dilatometer (Bähr VIS 404) installed at TU Clausthal consists of a SiO_2 rod subjected to a load (in this case 200 g, i.e. 1.96 N) pushing a sapphire sphere of radius r = 0.75 mm. The temperature was controlled with an S-type thermocouple (Pt-PtRh) placed at ~2 mm from the sample surface, resulting in an estimated error of ± 5 K. The accuracy of the instrument was confirmed by measuring the standard glass DGG-1, whose certified viscosity [41] was reproduced within an error of ±0.1 log units. Here, the sample was heated at 10 K min^{-1} up to 547 °C and then at 5 K min^{-1} up to the target measuring temperature of 645 °C. The measurement lasted ~3 h, with a minor gradual temperature increase to 647 °C. The penetration of the sapphire sphere was measured as a function of time using a linear variable displacement transducer, which was converted into viscosity according to the literature [42]. The sample is recalled in the following focussing on the viscosity values obtained at the beginning and at the end of the measurement, respectively as MP645start and MP645end. To associate a Raman spectrum with MP645start, the same time-temperature program used during the micropenetration experiment was applied in the above-mentioned DSC calorimeter (for practical reasons), cooling the glass sample to room temperature directly after reaching the temperature of 645 °C.

High-temperature viscosity data were acquired using a glass [29,30] previously synthesized by conventional melt-quenching with the same stoichiometry as the one prepared by ADL ($LiAlSi_2O_6$ + 4 mol% TiO_2). The measurements were performed with a Pt-Rh20 concentric cylinder viscometer, continuously monitoring viscosity during cooling from 1550 °C. The experiment was arrested at the onset of devitrification (at around 1210 °C, signaled by a sudden increase in viscosity).

2.4. Raman spectroscopy

The starting glass and all samples measured by DSC and micropenetration viscometry were characterized by Raman spectroscopy at TU Clausthal using an alpha300R spectrometer (WITec GmbH) equipped with a green diode laser (532 nm) and a CCD detector. The measurements were performed with 10 s acquisition time and 10 accumulations, after focusing several tens of micrometers below the sample surface.

High-temperature Raman spectroscopy characterization was performed at the FAU Erlangen-Nürnberg using the custom-made associated Raman-Brillouin-calorimeter (ARABICA) described in detail elsewhere [43], mounting a blue laser (488 nm) and enabling spectroscopic measurements in back-scattered geometry. At the same time, the sample is annealed in a PerkinElmer DSC 8500 modified by installing a SiO_2 glass window on its lid. In this work, a glass sphere was cut in half and one of the two hemispheres was placed in a Au crucible (with a hole in its lid to allow laser beam access). It was treated under N_2 flow in the DSC, according to the following time-temperature program: heating at 40 K min^{-1} to 640 °C; isothermal dwell for 6 h; cooling at 40 K min^{-1} to room temperature; short isothermal dwell (to check the sample and acquire a room temperature spectrum); heating at 40 K min^{-1} to 640 °C; isothermal dwell of 5 min; heating at 0.5 K min^{-1} to 660 °C; isothermal dwell of 10 h; cooling at 40 K min^{-1}. Raman measurements were performed continuously during the experiment, recursively acquiring signal over 4 minutes. After the experiment, the data were subjected to: (i) Raman shift correction based on a $CaCO_3$ standard; (ii) subtraction of the spectra collected in "dark" (closed detector) and in N_2 in the DSC to respectively remove undesired contributions to the baseline and artifacts at low wavenumber; (iii) manual despiking. For easier comparability, all spectra were normalized to the main Raman band associated with the aluminosilicate amorphous network, i.e. to the average intensity in the range 455–475 cm^{-1}.

3. Results

DSC upscans at 5 and 10 K min^{-1} were used to gain an overview of the crystallization sequence of the spodumene glass doped with 4 mol% TiO_2 synthesized by ADL (Fig. 1); further details about the crystalline phases and nanostructures that are obtainable in this composition are published elsewhere [29,30]. For comparison, a DSC curve previously recorded [30] at 2 K min^{-1} from a sample prepared by conventional melt-quenching is reported also here. Apart from an expected and consistent shift due to the different heating rates, the data exhibit outstanding agreement, supporting (together with the Raman data, see below) the successful synthesis of a glass with the target stoichiometry. In all measurements, three main thermal events were identifiable as the temperature increased, namely: (i) an endothermic step (best-visible at faster heating rates) corresponding to the relaxation into the supercooled liquid state, i.e. the glass transition (T_{glass}); (ii) TiO_2-driven seed formation (T_{seed}), partially overlapping with the previous thermal event and producing a broad exothermic peak, as already pointed out in previous works [19,20,30,44,45]; (iii) a sharper and more intense exothermic peak (T_{cryst}), which can be assigned to the volume crystallization of quartz solid solution crystals [27,29,30].

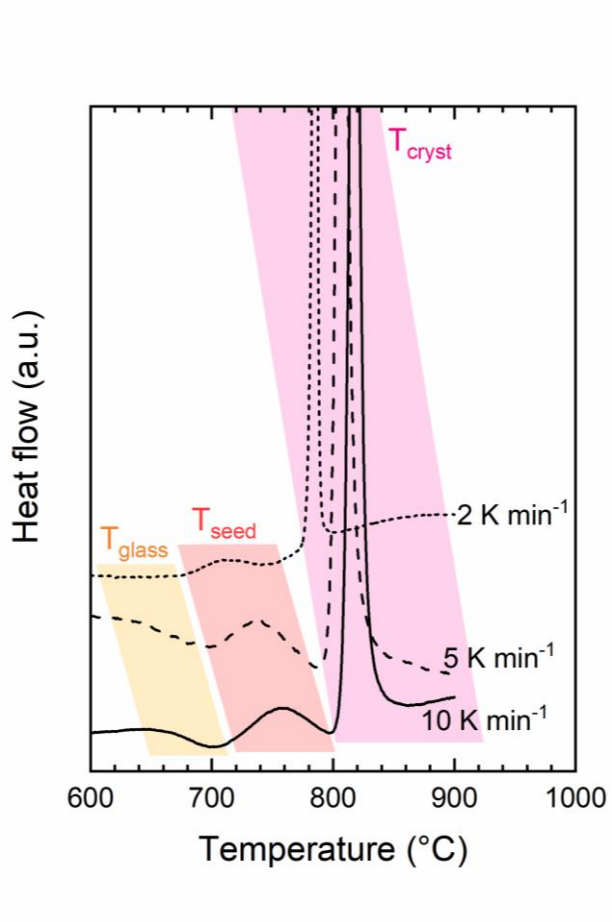

Figure 1. DSC upscans performed at a rate of 10 (continuous line), 5 (dashed line) or 2 K min^{-1} (dotted line, this latter from a previous work [30]) on spodumene glass doped with 4 mol% of TiO_2. Labels and color shadings mark the occurrence of a glass transition (T_{glass}), the formation of TiO_2 crystalline seeds (T_{seed}) and the volume crystallization of quartz solid solution crystals (T_{cryst}).

Based on the recorded calorimetry curves, we performed a micropenetration viscometry measurement at 645 °C to derive the viscosity of the sample in the temperature range of T_{glass}, i.e. possibly before the onset of T_{seed}. The results (Fig. 2) revealed a steady viscosity increase from 11.6(1) to 12.0(1) log Pa s during the measurement, which is not to be expected in stable glass formers and can be associated with phase separation or crystallization phenomena occurring in the material due to the high-temperature dwell [21,23]. The starting and final viscosity values recorded during the measurement are recalled and discussed in the following

under the respective labels MP645start and MP645end. To investigate the origin of such viscosity increase in higher detail, we therefore characterized the sample by high-temperature Raman spectroscopy in the same temperature range.

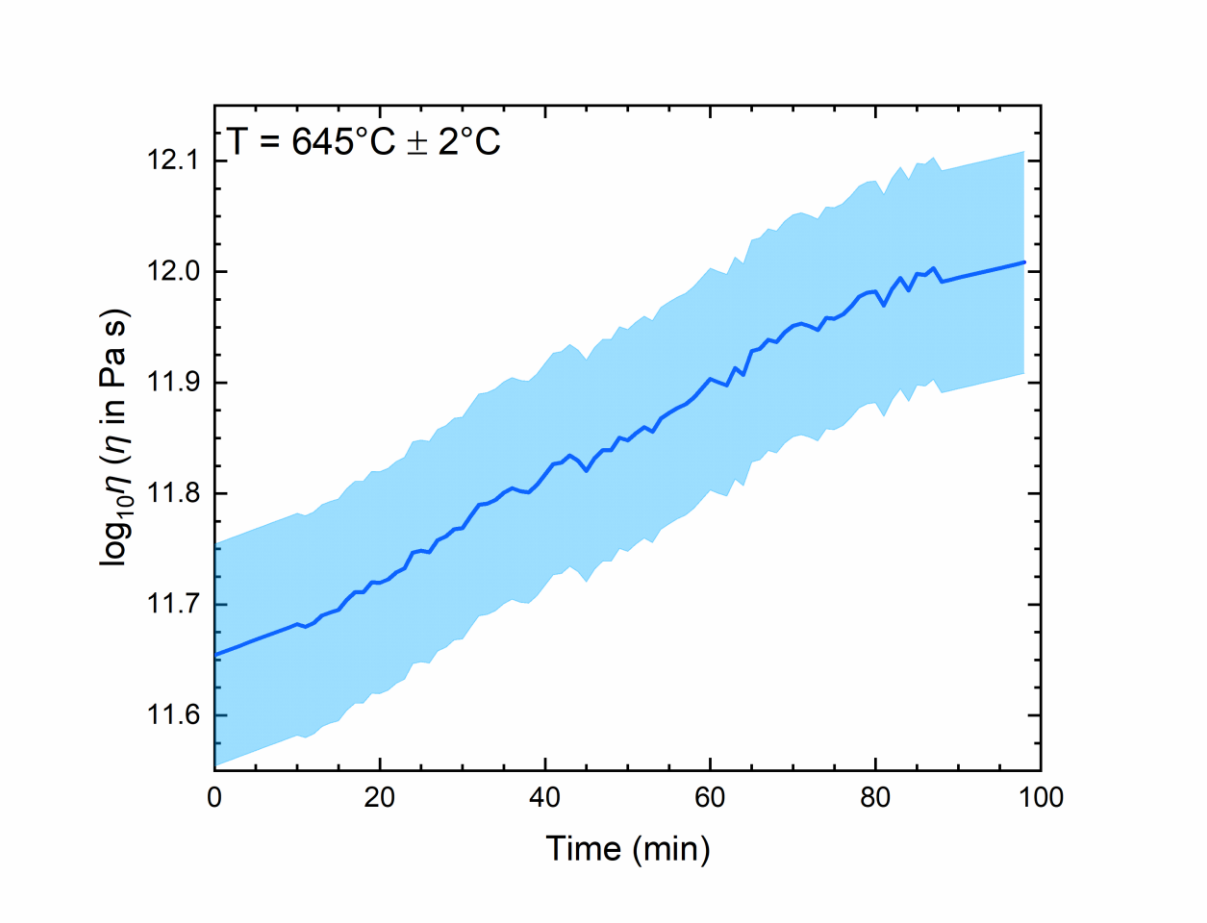

Figure 2. Results of a micropenetration viscometry measurement performed isothermally at 645 °C on a spodumene glass sample doped with 4 mol% TiO_2. The shaded area corresponds to the estimated uncertainty of the recorded values.

The Raman spectrum of the starting glass (Fig. 3-a) was in good agreement with those acquired previously from the same or similar compositions [27,29,46]. The most prominent spectral features included: (i) a broad asymmetric band with maximum at 480 cm^{-1}, corresponding to the vibrations of intertetrahedral linkages in the aluminosilicate network [46–48]; (ii) a broad local maximum centered around 900 cm^{-1} and associated with the incorporation of Ti^{4+} in the glassy network in the form of low-coordinated (4- and 5-fold) species

[20,21,29,49–51]. During the applied heating program involving two isothermal dwells at 640 °C and 660 °C, the Raman spectrum of the glass exhibited evident changes (Fig. 3-b): the intensity decreased above 800 cm^{-1}, while it increased below 250 cm^{-1} and around 600 cm^{-1} (especially at 660 °C). In these latter regions, the most intense Raman features of TiO_2 crystalline polymorphs are located, such as anatase, rutile, brookite and TiO_2(B), involving 6-fold oxygen coordination around Ti^{4+} (see for instance [29] and references therein). No Raman signatures assignable to aluminosilicate crystals (such as quartz or keatite solid solutions [29]) were identified. As such, the spectral changes can be attributed to a subtle structural relaxation occurring at 640 °C in the form of an amorphous phase separation, seemingly evolving at 660 °C into the formation of poorly ordered TiO_2 nanocrystals (size estimated based on the preserved transparency of the sample and on previous works [20,29]).

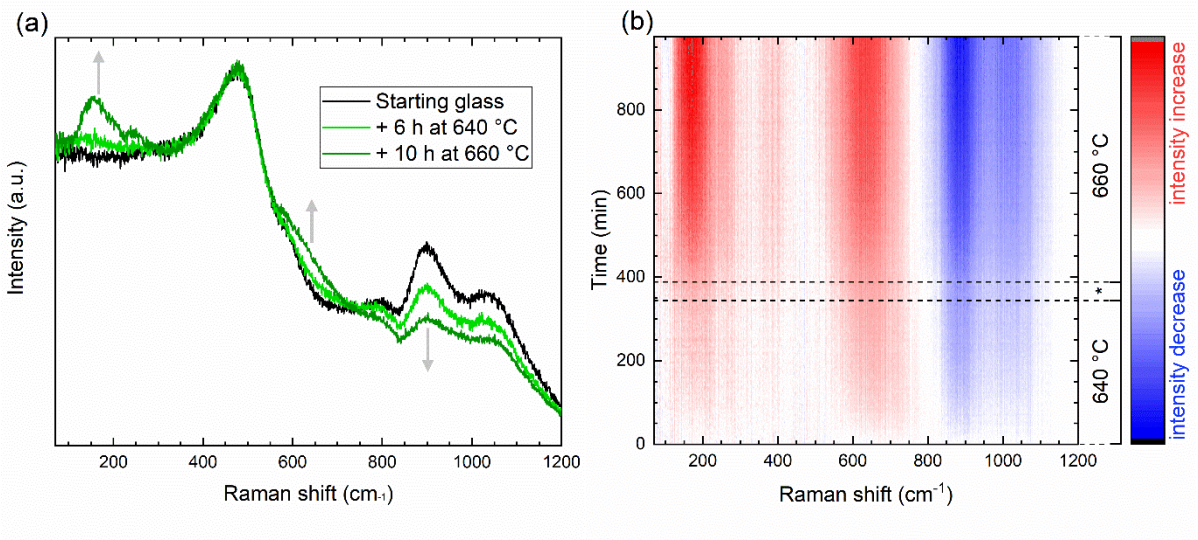

Figure 3. (a) Raman spectra acquired at room temperature from the starting TiO_2-doped spodumene glass, as well as after a dwell at 640 °C for 6 h and after an additional heat treatment at 660 °C for 10 h. (b) Color map manifesting intensity changes in the Raman spectra collected in-situ during the heat treatments at 640 °C and 660 °C (* marks the time spent by the sample in a heating ramp at 0.5 K min^{-1} between these two temperatures; spectra acquired during heating and cooling ramps at 40 K min^{-1} have been omitted for clarity).

Since micropenetration viscometry measurements exhibited a time-dependent increase in viscosity due to TiO_2 seed formation occurring in the sample in this temperature range (see also below), we additionally tested whether viscosity could be more reliably determined by a calorimetric approach. As described elsewhere and in Section 2.2 [21,34–36], this kind of analysis requires heating the glass through the glass transition to erase its previous thermal history, followed by cooling at a defined rate q_c and then by measuring its heat flow curve during re-heating at $q_h = q_c$. Due to the close overlap between T_{glass} and T_{seed} identified in Figure 1, we attempted to minimize the high-temperature exposure of the sample during the first heating cycle, comparing the results obtained using different maximum temperatures T_{max} and $q_h = q_c$ = 10 K min^{-1}. Clear changes in the shape of the heat flow curves could be observed between first and second heating segment (Fig. 4-a), manifesting some sort of material modification especially for the samples that reached the highest temperatures (10DSC733 and 10DSC759). Concerning the position of T_{onset}, it consistently shifted to higher temperature as T_{max} increased, by as much as 40 °C between 10DSC705 and 10DSC759. Further attempts using different heating rates (5 and 20 K min^{-1}) and a very limited high-temperature exposure were similarly unsuccessful, confirming the instability of the material under study: the obtained T_{onset} values scattered over a wide range (Fig. 4-b) and did not align on the typical linear trend exhibited by good glass formers on a logarithmic plot (measurements performed on the standard glass DGG-1 [34] are reported for comparison).

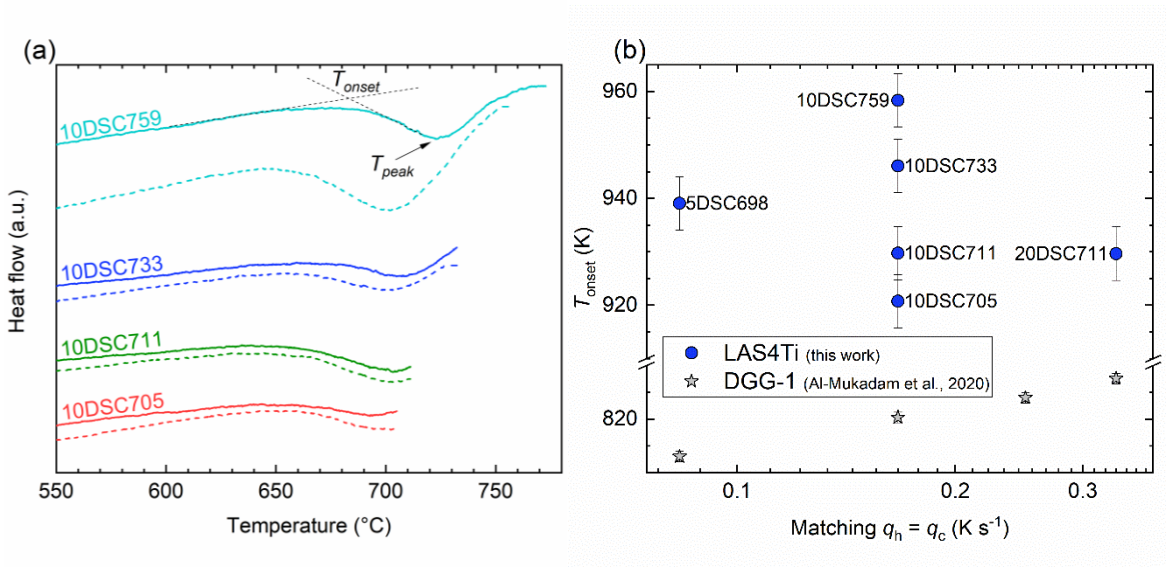

Figure 4. (a) DSC traces recorded during measurements of T_{onset} (the geometrical construction is exemplified for 10DSC759) on spodumene glass doped with 4 mol% TiO_2: dashed lines correspond to the first upscans performed at a rate of 10 K min^{-1} up to different maximum temperatures, followed by a cooling segment (not shown) and by a second upscan at the same rate (continuous line). (b) Correlation between T_{onset} values determined experimentally and the heating rate $q_h = q_c$ of the corresponding DSC run (horizontal axis in logarithmic scale); data previously measured on the standard DGG-1 glass [34] are reported for comparison.

We exploited again Raman spectroscopy to characterize the samples post-mortem, after viscosity or calorimetric measurements. To associate a Raman spectrum to the sample MP645start, we treated a glass chip with the same time-temperature program as the one used for the micropenetration experiment, without the isothermal hold at 645 °C. The spectra of all the measured samples differed clearly from that of the starting glass (Fig. 5-a), exhibiting analogous changes to those identified in Figure 3, that is an evident dwindling of the broad band centered at ~900 cm^{-1}, paralleled by rises in intensity at lower Raman shift. The additional intensity below 250 cm^{-1} and around 600 cm^{-1} distributed over a set of well-defined sharper bands in samples that reached the highest T_{max} (10DSC733 and 10DSC759), allowing their assignment to the formation of a mixture of crystalline anatase and TiO_2(B), as observed in

previous works [27,29]. As detailed in Figure 5-b, the ratio of the Raman intensities recorded at 480 and 900 cm^{-1} (I_{480}/I_{900}) gradually increased as the T_{max} achieved during the measurements increased (disregarding other differences in heating rate, heating cycles and isothermal dwell). This correlation manifests the "exit" of low-coordinated Ti^{4+} from the aluminosilicate melt structure during phase separation through the formation of TiO_2 nanocrystals (size estimated based on the preserved transparency of the sample and on previous works [20,29]).

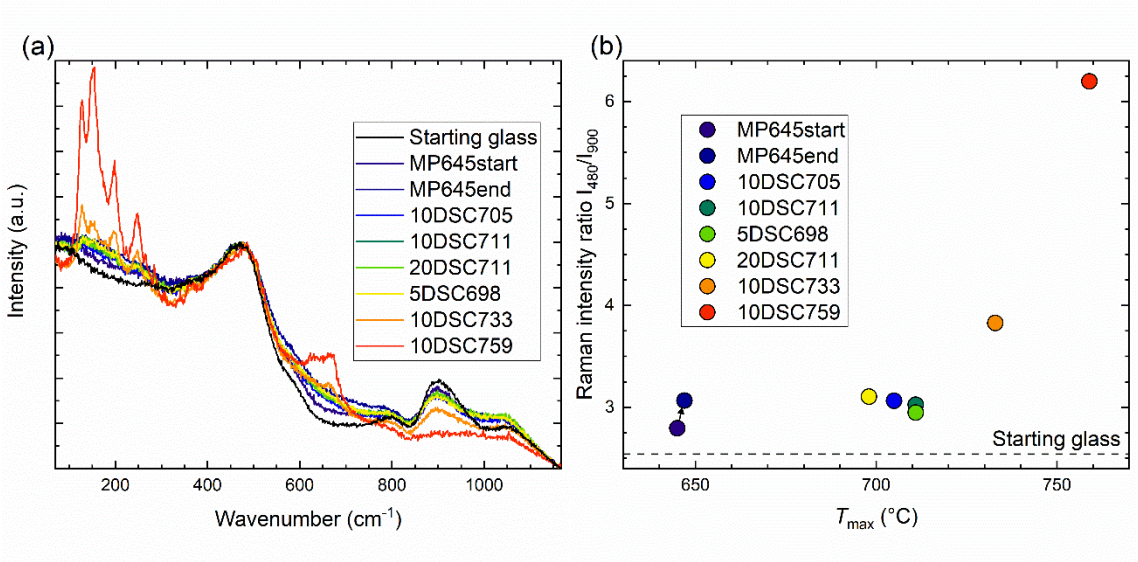

Figure 5. (a) Raman spectra (excitation at 532 nm) collected from samples previously subjected to micropenetration viscometry and DSC measurements, as well as from the untreated starting glass. (b) Correlation between the Raman intensity ratio I_{480}/I_{900} and the maximum temperature T_{max} achieved by the respective samples during viscosity or calorimetry measurements, disregarding other differences in heating rate, heating cycles and isothermal dwell.

4. Discussion

4.1 Seed formation and crystallization of TiO_2-doped spodumene glass

As a model sample, spodumene glass doped with 4 mol% TiO_2 perfectly exemplifies the expected behaviour of glass-ceramics containing seed formers, and particularly of low-thermal expansion glass-ceramics [52]. Its simplified composition exhibits markedly lower

glass-forming ability than commercial products, so that glass can be reliably synthesized only in small amounts, using techniques enabling comparatively high cooling rates such as roller-quenching or containerless processing [27,29,30]. However, its crystallization sequence recalls very closely the stages that are usually encountered in the two-step ceramization of industrial glass-ceramics [2], as schematized in Figure 6.

As demanded by a recently updated definition of glass [2], heating the TiO_2-doped spodumene glass clearly produces a first relaxation step into the supercooled liquid state, which was labelled as T_{glass} on heat flow curves (Fig. 1). Nevertheless, structural relaxation seems to be indissolubly connected to compositional rearrangements at the nanoscale, which occur almost simultaneously and initiate the phase separation of amorphous TiO_2-enriched droplets, as evidenced in previous works [19,53] and inferred here by Raman spectroscopy. The driving force for chemical diffusion can be identified in the poor solubility of transition metal cations in deeply supercooled silicate melts (as recently postulated for basalts [23]). Although viscosity is still very high in the vicinity of T_g, the mobility of single chemical species was shown to exceed approximations based on Stokes–Einstein assumptions [7], markedly decoupling from cooperative atomic movements at these temperatures. The analysis of tracers diffusion in a TiO_2-doped albite glass [54] newly demonstrated that the diffusivities of Ti^{4+} and Al^{3+} are very similar at deep undercooling and close to the one of O^{2-}, while the mobility of Al^{3+} is lower by orders of magnitude in the absence of TiO_2. Such observation can be linked to the frequent observation of Al^{3+}-enriched shells around TiO_2 crystal nuclei in glasses and glass-ceramics [18,20,21,29], supporting the key role of seed formers in inducing pervasive nanostructural modifications of the residual glass during diffusion processes leading to phase separation and nucleation.

Following a non-classical path [55], crystal nucleation is then observed only after the local composition has already achieved that of the phase to be formed, i.e. pure TiO_2. The energetic demand to achieve long-range ordering is minimized by the precipitation of

metastable polymorphs such as TiO_2(B) and anatase [29,56], which represent, also because of their nanosize, favourable intermediates to the final precipitation of rutile (at around 1000 °C, see [30]) according to Ostwald's rule of stages [57]. Eventually, heat treatments trigger also devitrification of the residual lithium aluminosilicate amorphous matrix, which occurs in a controlled fashion through heterogeneous nucleation on the existing TiO_2 seeds [29,30]. The role of the nucleating agents is therefore to catalyse the uniform volume crystallization of functional quartz solid solution crystals with negative thermal expansion [58] through structural [59] or chemical epitaxy at the compositional gradients surrounding the TiO_2 nuclei [18,20,29]. Although the crystallization is typically arrested at this stage, it is important to note that quartz solid solutions are themselves metastable at spodumene composition, acting as metastable precursors for the formation of thermodynamically stable keatite solid solution crystals [30,60] (also called β-spodumene in previous literature).

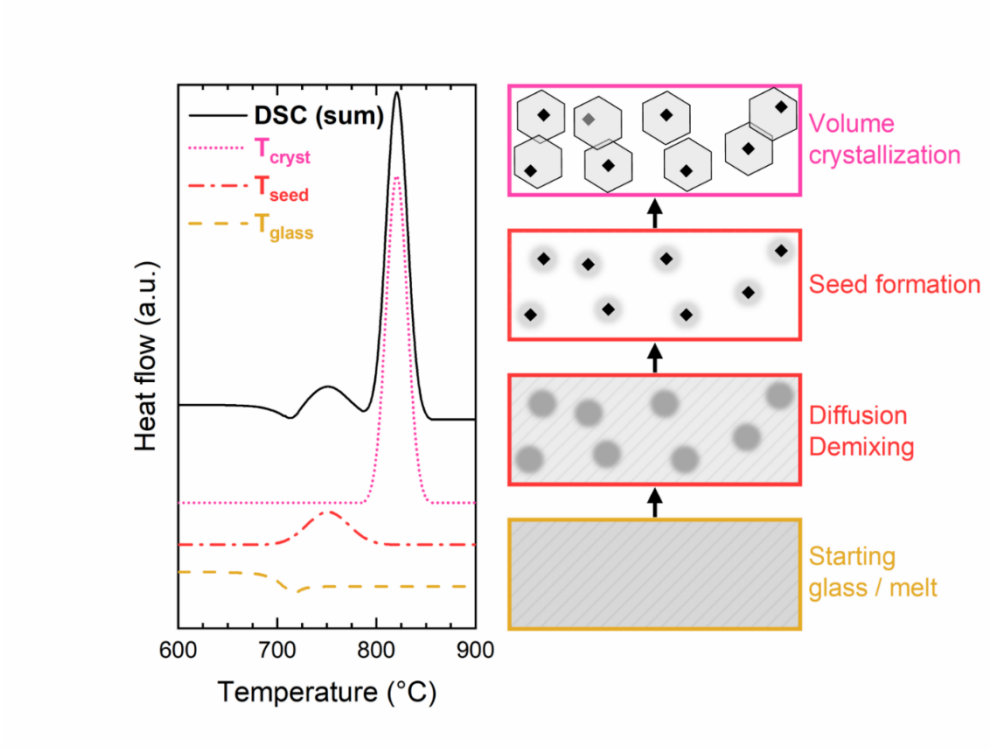

Figure 6. A schematic summary of the crystallization mechanism of spodumene glass doped with 4 mol% TiO_2, identifying the main processes that are typically observed during a (hypothetical) DSC heating experiment. The assumedly homogeneous starting glass undergoes

relaxation into the supercooled liquid state; almost simultaneously, its structure begins to undergo medium-range rearrangement through chemical diffusion and subsequent phase separation. TiO_2 nanocrystals can then precipitate in areas that are enriched in the transition metal oxide, eventually fostering the heterogeneous nucleation of quartz solid solution crystals by chemical and/or structural epitaxy.

4.2 Implications for viscosity measurements and full-curve parameterization

Our results manifest the experimental challenges related to accurately measuring the viscosity of supercooled melts that are supersaturated in one of their oxide components, such as the parent melts of glass-ceramics containing seed formers. These materials can only be quenched into glasses at comparatively fast cooling rates, hindering chemical processes (chemical diffusion, crystal nucleation and growth) that are inevitably initiated by the supercooling. A driving force towards crystallization exists however even during a fleeting permanence at temperatures lower than the melting point T_m and cannot be completely suppressed even at cooling rates of hundreds (or thousands) of K min^{-1}. Especially for melts that do not undergo stoichiometric crystallization, the effects of such metastability were previously identified as ZrO_2-rich nanoscale heterogeneities (assimilable to an incipient phase separation) in as-quenched glasses [61]. Although the kinetics of chemical diffusion, crystal nucleation and growth in silicate glasses can be considered negligible at room temperature, these processes are readily reactivated by heating through the glass transition region and beyond. Therefore, any viscosity measurements will have to face and minimize possible inaccuracies caused by the above-mentioned temperature-activated processes, particularly considering that the experiments performed in this work demonstrate that structural relaxation and seed formation occur over very similar timescales in melts containing seed formers such as TiO_2.

While the influence of melt devitrification at shallow supercooling is easy to notice (crystal growth is fast in these conditions, leading to abrupt changes in the rheological response), material modifications are more subtle and therefore less controllable at deep supercooling, as shown in this and previous works [21,23]. In the following, we will exemplarily demonstrate the repercussions that inaccurate viscosity measurements (due to near-T_g non-stoichiometric crystallization) can have on a viscosity parameterization performed by fitting low- and high-temperature data, the latter measured by concentric-cylinder (CC) rheometry. In addition to the DSC and micropenetration data discussed in the Results section, we also measured the heat flow of the TiO_2-doped spodumene glass by FDSC at q_h=q_c 1000 K s^{-1} to extract the temperature (T_{onset}) at which $\log_{10}\eta$ = 8.2 log Pa s (pink star on Fig. 7-a) through Equation 1. The data were fitted using the MYEGA formulation [12], that is (Eq. 2):

$$log_{10}\eta = log_{10}\eta_\infty + (12 - log_{10}\eta_\infty)\frac{T_g}{T} exp\left[\left(\frac{m}{12-log_{10}\eta_\infty} - 1\right)\left(\frac{T_g}{T} - 1\right)\right] \qquad \text{(Eq. 2)}$$

where $\log_{10}\eta_\infty$, T_g and m are three independent fit parameters, namely the viscosity at the limit of infinite temperature, the glass transition temperature (where η = 10^{12} Pa s) and the melt fragility, defined as the slope of the curve evaluated at T_g, i.e. (Eq. 3):

$$m = \left.\frac{\partial log_{10}\eta(T)}{\partial\left(\frac{T_g}{T}\right)}\right|_{T=T_g} \qquad \text{(Eq. 3)}$$

As shown in Figure 7-a, low-temperature data scattered over a wide range of temperature and viscosity values, due to their different crystallization degrees demonstrated in Figure 5. We therefore decided to treat each low-temperature point as a separate dataset, obtaining 9 possible parameterizations for the viscosity of a spodumene melt doped with 4 mol% TiO_2 (Tab. 1). All fits exhibited very high R^2 and their fitting parameters converged to

reasonable values, i.e. the quality of the MYEGA parameterizations was virtually unperturbed even when using data obtained from highly crystallized samples such as 10DSC733 and 10DSC759. As a matter of fact, it would be impossible to infer measurement inaccuracies at this stage of the analysis, without the careful Raman characterization presented above. Due to the strong constraint provided by CC data, all curves superimposed in the range 1500–1800 K but increasingly diverged at lower temperature and at the limit of infinite temperature. A mutual correlation between the fitting parameters was clearly visible: T_g and m increased in parallel, respectively from 898.3(3) K and 31.2(1) for FDSC to 957.7(2) K and 37.9(1) for 10DSC759; at the same time, $\log_{10}\eta_\infty$ increased from -3.29(1) to -2.23(1), gradually wandering away the universal high-temperature viscosity limit previously extrapolated to -2.9(3) log Pa s [62,63]. According to the chosen dataset, we therefore obtained T_g values differing by as much as ~60 K. Considering a given temperature such as 950 K, the calculated viscosity values differ by as much as ~2 log units between the $10^{12.3}$ Pa s of 10DSC759 and the $10^{10.3}$ Pa s of FDSC, with only minimal variations in the thermal history of the samples.

Table 1. Parameters obtained from viscosity fits based on the MYEGA equation, performed using high-temperature CC data and, alternatively, near-T_g datapoints obtained from each of the samples measured within this work by (F)DSC or micropenetration viscometry. The data is ordered by increasing T_g parameter.

Sample	T_g (K)	m	$\log_{10}\eta_\infty$ (η in Pa s)	R^2
FDSC	898.3(3)	31.2(1)	-3.29(1)	0.99998
MP645start	908.1(1)	32.2(1)	-3.11(1)	0.99998
10DSC705	920.1(1)	33.5(1)	-2.89(1)	0.99997
20DSC711	920.6(2)	33.5(1)	-2.88(1)	0.99997

MP645end	921.6(2)	33.7(1)	-2.87(1)	0.99997
10DSC711	929.1(2)	34.5(1)	-2.73(1)	0.99996
10DSC733	945.4(2)	36.4(1)	-2.44(1)	0.99993
5DSC698	946.1(2)	36.5(1)	-2.43(1)	0.99993
10DSC759	957.7(2)	37.9(1)	-2.23(1)	0.99990

It is clear that only one of the obtained MYEGA parameterizations provides the correct viscosity of a homogeneous spodumene melt containing 4 mol% TiO_2 (or its closest approximation), while all other curves represent an erroneous parameterization affected by phase separation and crystallization occurring in the starting material during low-temperature measurements. Highly crystallized samples such as 10DSC733 and 10DSC759 plotted intriguingly close to the viscosity of a TiO_2-free spodumene melt from literature [15] (dashed black line in Fig. 7): this is expected from samples that experienced partial TiO_2 removal from their melt structure due to the precipitation of anatase and TiO_2(B), gradually approaching a TiO_2-free residual melt composition [20,21,27]. Also the evident correlation between *m* indices and the I_{480}/I_{900} of the respective specimens (Fig. 7-b) confirms that differences between the samples should be attributed to the decreasing TiO_2 content of their residual melt phase, and not (or at least not primarily) to a contrasting or insufficient degree of melt relaxation achieved during the measurements.

While calorimetric measurements directly investigate the viscosity of the residual melt (the only phase exhibiting a glass transition) during its crystallization-driven compositional evolution, micropenetration measurements should effectively picture the rheology of the whole system (melt+crystals). Existing models [14,64] predict no influence on viscosity from 1-2 vol% nanocrystals and the results obtained here are in good agreement with such assumptions. Nevertheless, micropenetration viscometry was performed here on a sample exhibiting only limited modifications (no crystals are visible on the Raman spectrum of MP645end in Fig. 5);

therefore, previous speculations on the overproportional increase in the effective viscosity of highly heterogeneous nanocrystallized melts [21] reach beyond the scope of this study and still deserve further investigation.

Following the above-presented line of reasoning, the correct viscosity (or its closest approximation) of the TiO_2-bearing starting glass should correspond to the lowest obtained values, i.e. to the fits performed using MP645start or FDSC. MP645start was heated to the lowest T_{max} among all samples and exhibited the most similar Raman spectrum to the one of the starting glass (Fig. 5). However, the variation of its I_{480}/I_{900} is still significant within the trend defined by the other samples as a function of m (Fig. 7-b), manifesting a certain degree of material modification. The overall trend in Fig. 7-b converges instead towards the intercept between the I_{480}/I_{900} of the initial glass and the m of the FDSC fit (the two dashed lines in figure 7-b), supporting the accuracy of this latter parameterization to describe the viscosity of a spodumene melt doped with 4 mol% TiO_2. Indeed, the permanence of the FDSC sample at high temperatures accounted to only few fractions of a second, effectively preventing undesired extensive chemical diffusion during the measurements. Despite its challenging requirements and the need to perform several measurements to ensure reproducibility, FDSC was also recently shown to be a very powerful tool to investigate the crystal-free viscosity of unstable melts that are prone to non-stoichiometric crystallization during experiments [40]. All in all, the results of this work consolidate the validity of a recently presented vademecum for the experimental investigation of the viscosity of unstable samples [23], suggesting a minimization of the high-temperature exposure during measurements and the use of Raman spectroscopy (or TEM) to evaluate material modifications possibly invalidating the results.

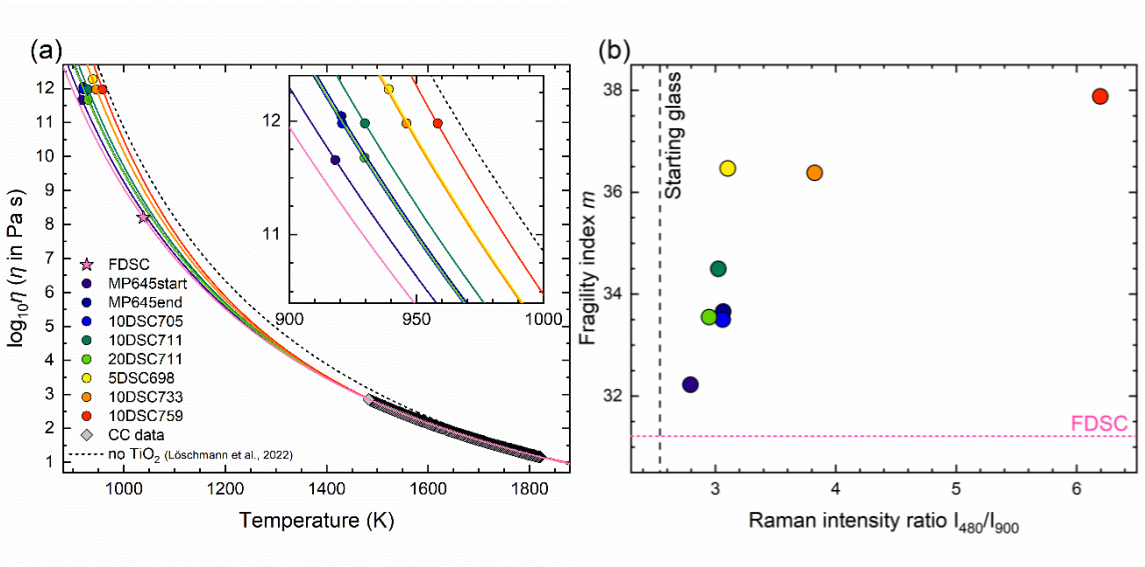

Figure 7. (a) Viscosity curves obtained by fitting the MYEGA equation to high-temperature concentric-cylinder (CC) data and, alternatively, one of the low-temperature datapoints obtained by (F)DSC and micropenetration viscometry. A dashed line represents the viscosity trend of a TiO_2-free spodumene melt, as obtained from literature [15]. The closest approximation to the real viscosity of a homogeneous spodumene melt containing 4 mol% TiO_2 is provided by the fit obtained from sample FDSC. (b) Correlation between the fragility indices *m* resulting from MYEGA fitting and the Raman intensity ratio I_{480}/I_{900} of the respective samples; a vertical dashed line localizes the value of I_{480}/I_{900} for the starting glass, while a horizontal dotted line corresponds to the *m* of the fit performed on the base of a FDSC datapoint.

5. Conclusions

Glass-ceramics containing seed formers are designed to undergo early phase separation and/or crystal nucleation during heat treatments, making viscosity measurements of their homogeneous parent melt a tough challenge. As demonstrated here, viscosity deviations by up to 2 orders of magnitude can arise from inattentive experiments, which may severely affect the ability to control viscous deformation during crystallization heat treatments for glass-ceramic manufacturing. Although it is difficult to define an ever-valid experimental procedure to circumvent such problems and reliably determine the viscosity of the homogeneous parent melt,

it is possible to minimize errors by limiting high-temperature exposure during measurements and performing a careful post-mortem evaluation of measured samples using suitable analytical tools.

Acknowledgements

AZ is grateful to the Deutsche Forschungsgemeinschaft (DFG) for funding his research through the Walter Benjamin Program, project n. 448961237, ZA 1188/1-1 and ZA 1188/2-1. DDG, JL and JD acknowledge funding by DFG projects DI 2751/2–1 and DE 598/33-1. DDG acknowledges the funding from the European Research Council (ERC) under the European Union's Horizon Europe research and innovation programme (NANOVOLC, ERC Consolidator Grant – No. 101044772). AS, FDF and AV acknowledge the Grant of Excellence Departments, MIUR-Italy (ARTICOLO 1, COMMI 314 - 337 LEGGE 232/ 2016). The authors would like to acknowledge Marion Kalden for performing concentric-cylinder viscosity measurements and the company Schott AG for providing these data.

References

[1] J.D. Musgraves, J. Hu, L. Calvez, eds., Springer Handbook of Glass, Springer, 2019.
[2] J. Deubener, M. Allix, M.J. Davis, A. Duran, T. Höche, T. Honma, T. Komatsu, S. Krüger, I. Mitra, R. Müller, S. Nakane, M.J. Pascual, J.W.P. Schmelzer, E.D. Zanotto, S. Zhou, Updated definition of glass-ceramics, Journal of Non-Crystalline Solids. 501 (2018) 3–10. https://doi.org/10.1016/j.jnoncrysol.2018.01.033.
[3] M. Montazerian, S.P. Singh, E.D. Zanotto, An analysis of glass-ceramics research and commercialization, American Ceramic Society Bulletin. 94 (2015) 30–35.
[4] G.H. Beall, Design and Properties of Glass-Ceramics, Annu. Rev. Mater. Sci. 22 (1992) 91–119. https://doi.org/10.1146/annurev.ms.22.080192.000515.
[5] R. Laniel, M. Hubert, M. Miroir, A. Brient, Glass Shaping, in: J.D. Musgraves, J. Hu, L. Calvez (Eds.), Springer Handbook of Glass, Springer International Publishing, Cham, 2019: pp. 1259–1292. https://doi.org/10.1007/978-3-319-93728-1_36.
[6] M. Hubert, Industrial Glass Processing and Fabrication, in: J.D. Musgraves, J. Hu, L. Calvez (Eds.), Springer Handbook of Glass, Springer International Publishing, Cham, 2019: pp. 1195–1231. https://doi.org/10.1007/978-3-319-93728-1_34.
[7] M.L.F. Nascimento, E. Dutra Zanotto, Does viscosity describe the kinetic barrier for crystal growth from the liquidus to the glass transition?, J. Chem. Phys. 133 (2010) 174701. https://doi.org/10.1063/1.3490793.

[8] H. Vogel, Das Temperaturabhängigkeitsgesetz der Viskosität von Flüssigkeiten, Physikalische Zeitschrift. 22 (1921) 645.
[9] G.S. Fulcher, ANALYSIS OF RECENT MEASUREMENTS OF THE VISCOSITY OF GLASSES, Journal of the American Ceramic Society. 8 (1925) 339–355. https://doi.org/10.1111/j.1151-2916.1925.tb16731.x.
[10] G. Tammann, W. Hesse, Die Abhängigkeit der Viscosität von der Temperatur bie unterkühlten Flüssigkeiten, Zeitschrift Für Anorganische Und Allgemeine Chemie. 156 (1926) 245–257. https://doi.org/10.1002/zaac.19261560121.
[11] G. Adam, J.H. Gibbs, On the Temperature Dependence of Cooperative Relaxation Properties in Glass-Forming Liquids, The Journal of Chemical Physics. 43 (1965) 139–146. https://doi.org/10.1063/1.1696442.
[12] J.C. Mauro, Y. Yue, A.J. Ellison, P.K. Gupta, D.C. Allan, Viscosity of glass-forming liquids, Proceedings of the National Academy of Sciences. 106 (2009) 19780–19784. https://doi.org/10.1073/pnas.0911705106.
[13] M.L.F. Nascimento, L.A. Souza, E.B. Ferreira, E.D. Zanotto, Can glass stability parameters infer glass forming ability?, Journal of Non-Crystalline Solids. 351 (2005) 3296–3308. https://doi.org/10.1016/j.jnoncrysol.2005.08.013.
[14] Z. Liu, L. Pandelaers, B. Blanpain, M. Guo, Viscosity of Heterogeneous Silicate Melts: A Review, Metallurgical and Materials Transactions B. 49 (2018) 2469–2486. https://doi.org/10.1007/s11663-018-1374-9.
[15] J. Löschmann, P. Fielitz, G. Helsch, H. Bornhöft, D.R. Cassar, G. Borchardt, J. Deubener, Accelerated crystal growth in a lithia aluminosilicate glass, Acta Materialia. 230 (2022) 117837. https://doi.org/10.1016/j.actamat.2022.117837.
[16] U. Fotheringham, R. Wurth, C. Rüssel, Thermal analyses to assess diffusion kinetics in the nano-sized interspaces between the growing crystals of a glass ceramics, Thermochimica Acta. 522 (2011) 144–150. https://doi.org/10.1016/j.tca.2011.03.023.
[17] P. Fielitz, D.R. Cassar, N.S. Yuritsyn, A.S. Abyzov, V.M. Fokin, G. Borchardt, J. Deubener, Decelerated crystal growth in a soda-lime-silica glass, Journal of Non-Crystalline Solids. 596 (2022) 121879. https://doi.org/10.1016/j.jnoncrysol.2022.121879.
[18] S. Bhattacharyya, T. Höche, J.R. Jinschek, I. Avramov, R. Wurth, M. Müller, C. Rüssel, Direct Evidence of Al-Rich Layers around Nanosized ZrTiO4 in Glass: Putting the Role of Nucleation Agents in Perspective, Crystal Growth & Design. 10 (2010) 379–385. https://doi.org/10.1021/cg9009898.
[19] E. Kleebusch, C. Patzig, T. Höche, C. Rüssel, The evidence of phase separation droplets in the crystallization process of a Li2O-Al2O3-SiO2 glass with TiO2 as nucleating agent – An X-ray diffraction and (S)TEM-study supported by EDX-analysis, Ceramics International. 44 (2018) 2919–2926. https://doi.org/10.1016/j.ceramint.2017.11.040.
[20] A. Zandona, C.B.M. Groß, B. Rüdinger, J. Deubener, A threshold heating rate for single-stage heat treatments in glass-ceramics containing seed formers, Journal of the American Ceramic Society. 104 (2021) 4433–4444. https://doi.org/10.1111/jace.17822.
[21] D. Di Genova, A. Zandona, J. Deubener, Unravelling the effect of nano-heterogeneity on the viscosity of silicate melts: Implications for glass manufacturing and volcanic eruptions, Journal of Non-Crystalline Solids. 545 (2020) 120248. https://doi.org/10.1016/j.jnoncrysol.2020.120248.
[22] D. Di Genova, R.A. Brooker, H.M. Mader, J.W.E. Drewitt, A. Longo, J. Deubener, D.R. Neuville, S. Fanara, O. Shebanova, S. Anzellini, F. Arzilli, E.C. Bamber, L. Hennet, G. La Spina, N. Miyajima, In situ observation of nanolite growth in volcanic melt: A driving force for explosive eruptions, Science Advances. 6 (2020). https://doi.org/10.1126/sciadv.abb0413.
[23] A. Scarani, A. Zandonà, F. Di Fiore, P. Valdivia, R. Putra, N. Miyajima, H. Bornhöft, A. Vona, J. Deubener, C. Romano, D. Di Genova, A chemical threshold controls

nanocrystallization and degassing behaviour in basalt magmas, Communications Earth & Environment. 3 (2022) 284. https://doi.org/10.1038/s43247-022-00615-2.
[24] P. Stabile, S. Sicola, G. Giuli, E. Paris, M.R. Carroll, J. Deubener, D. Di Genova, The effect of iron and alkali on the nanocrystal-free viscosity of volcanic melts: A combined Raman spectroscopy and DSC study, Chemical Geology. 559 (2021) 119991. https://doi.org/10.1016/j.chemgeo.2020.119991.
[25] F.D. Fiore, A. Vona, A. Costa, S. Mollo, C. Romano, Quantifying the influence of cooling and shear rate on the disequilibrium rheology of a trachybasaltic melt from Mt. Etna, Earth and Planetary Science Letters. 594 (2022) 117725. https://doi.org/10.1016/j.epsl.2022.117725.
[26] F. Cáceres, F.B. Wadsworth, B. Scheu, M. Colombier, C. Madonna, C. Cimarelli, K.-U. Hess, M. Kaliwoda, B. Ruthensteiner, D.B. Dingwell, Can nanolites enhance eruption explosivity?, Geology. 48 (2020) 997–1001. https://doi.org/10.1130/G47317.1.
[27] A. Zandonà, S. Ory, C. Genevois, E. Véron, A. Canizarès, M.J. Pitcher, M. Allix, Glass formation and devitrification behavior of alkali (Li, Na) aluminosilicate melts containing TiO2, Journal of Non-Crystalline Solids. 582 (2022) 121448. https://doi.org/10.1016/j.jnoncrysol.2022.121448.
[28] A. Zandonà, M. Moustrous, C. Genevois, E. Véron, A. Canizarès, M. Allix, Glass-forming ability and ZrO2 saturation limits in the magnesium aluminosilicate system, Ceramics International. 48 (2022) 8433–8439. https://doi.org/10.1016/j.ceramint.2021.12.051.
[29] A. Zandona, C. Patzig, B. Rüdinger, O. Hochrein, J. Deubener, TiO2(B) nanocrystals in Ti-doped lithium aluminosilicate glasses, Journal of Non-Crystalline Solids: X. 2 (2019) 100025. https://doi.org/10.1016/j.nocx.2019.100025.
[30] A. Zandona, B. Rüdinger, O. Hochrein, J. Deubener, Crystallization sequence within the keatite solid solution – cordierite mixed compositional triangle with TiO2 as nucleating agent, Journal of Non-Crystalline Solids. 505 (2019) 320–332. https://doi.org/10.1016/j.jnoncrysol.2018.11.012.
[31] H. Bazzaoui, C. Genevois, E. Véron, M.J. Pitcher, M. Allix, A. Zandonà, Towards new zero-thermal-expansion materials: Li-free quartz solid solutions stuffed with transition metal cations, Journal of the European Ceramic Society. (2022). https://doi.org/10.1016/j.jeurceramsoc.2022.11.035.
[32] J. Baborák, M. Yembele, P. Vařák, S. Ory, E. Véron, M.J. Pitcher, M. Allix, P. Nekvindová, A. Zandonà, Key melt properties for controlled synthesis of glass beads by aerodynamic levitation coupled to laser heating, International Journal of Applied Glass Science. n/a (2023). https://doi.org/10.1111/ijag.16627.
[33] R. Al-Mukadam, A. Zandona, J. Deubener, Kinetic fragility of pure TeO2 glass, Journal of Non-Crystalline Solids. 554 (2021) 120595. https://doi.org/10.1016/j.jnoncrysol.2020.120595.
[34] R. Al-Mukadam, D. Di Genova, H. Bornhöft, J. Deubener, High rate calorimetry derived viscosity of oxide melts prone to crystallization, Journal of Non-Crystalline Solids. 536 (2020) 119992. https://doi.org/10.1016/j.jnoncrysol.2020.119992.
[35] G.W. Scherer, Use of the Adam-Gibbs Equation in the Analysis of Structural Relaxation, Journal of the American Ceramic Society. 67 (1984) 504–511. https://doi.org/10.1111/j.1151-2916.1984.tb19643.x.
[36] Y. Yue, R. von der Ohe, S.L. Jensen, Fictive temperature, cooling rate, and viscosity of glasses, J. Chem. Phys. 120 (2004) 8053–8059. https://doi.org/10.1063/1.1689951.
[37] R. Al-Mukadam, I.K. Götz, M. Stolpe, J. Deubener, Viscosity of metallic glass-forming liquids based on Zr by fast-scanning calorimetry, Acta Materialia. 221 (2021) 117370. https://doi.org/10.1016/j.actamat.2021.117370.

[38] M. Mancini, M. Sendova, J.C. Mauro, Geometric analysis of the calorimetric glass transition and fragility using constant cooling rate cycles, International Journal of Applied Glass Science. 12 (2021) 348–357. https://doi.org/10.1111/ijag.16073.
[39] A. Scarani, A. Vona, D. Di Genova, R. Al-Mukadam, C. Romano, J. Deubener, Determination of cooling rates of glasses over four orders of magnitude, Contributions to Mineralogy and Petrology. 177 (2022) 35. https://doi.org/10.1007/s00410-022-01899-5.
[40] D.D. Genova, D. Bondar, A. Zandonà, P. Valdivia, R. Al-Mukadam, H. Fei, A.C. Withers, T.B. Ballaran, A. Kurnosov, C. McCammon, J. Deubener, T. Katsura, Viscosity of anhydrous and hydrous peridotite melts, Chemical Geology. (2023) 121440. https://doi.org/10.1016/j.chemgeo.2023.121440.
[41] G. Meerlender, Viskositäts-Temperatur-Verhalten des Standardglases I der DGG, Glastechnische Berichte. 1 (1974) 1–3.
[42] R. Douglas, W. Armstrong, J. Edward, D. Hall, A penetration viscometer, Glass Technology. 6 (1965) 52–55.
[43] A. Veber, M.R. Cicconi, H. Reinfelder, D. de Ligny, Combined Differential scanning calorimetry, Raman and Brillouin spectroscopies: A multiscale approach for materials investigation, Analytica Chimica Acta. 998 (2018) 37–44. https://doi.org/10.1016/j.aca.2017.09.045.
[44] M. Dressler, B. Rüdinger, J. Deubener, Crystallization kinetics in a lithium alumosilicate glass using SnO2 and ZrO2 additives, Journal of Non-Crystalline Solids. 389 (2014) 60–65. https://doi.org/10.1016/j.jnoncrysol.2014.02.008.
[45] Q. Fu, B.R. Wheaton, K.L. Geisinger, A.J. Credle, J. Wang, Crystallization, Microstructure, and Viscosity Evolutions in Lithium Aluminosilicate Glass-Ceramics, Frontiers in Materials. 3 (2016) 49. https://doi.org/10.3389/fmats.2016.00049.
[46] S.K. Sharma, B. Simons, Raman study of crystalline polymorphs and glasses of spodumene composition quenched from various pressures, American Mineralogist. 66 (1981) 118–126.
[47] F.L. Galeener, A.E. Geissberger, Vibrational dynamics in 30Si-substituted vitreous SiO2, Physical Review B. 27 (1983) 6199–6204.
[48] F.L. Galeener, J.C. Mikkelsen, Vibrational dynamics in O18 -substituted vitreous SiO2, Phys. Rev. B. 23 (1981) 5527–5530. https://doi.org/10.1103/PhysRevB.23.5527.
[49] A. Zandonà, E. Chesneau, G. Helsch, A. Canizarès, J. Deubener, V. Montouillout, F. Fayon, M. Allix, Glass-forming ability and structural features of melt-quenched and gel-derived SiO2-TiO2 glasses, Journal of Non-Crystalline Solids. 598 (2022) 121967. https://doi.org/10.1016/j.jnoncrysol.2022.121967.
[50] G.S. Henderson, M.E. Fleet, The structure of Ti silicate glasses by micro-Raman spectroscopy, The Canadian Mineralogist. 33 (1995) 399–408.
[51] O.S. Dymshits, A.A. Zhilin, V.I. Petrov, M.Ya. Tsenter, T.I. Chuvaeva, V.V. Golubkov, A Raman spectroscopic study of phase transformations in titanium-containing lithium aluminosilicate glasses, Glass Physics and Chemistry. 24 (1998) 79–96.
[52] W. Pannhorst, Overview, in: H. Bach (Ed.), Low Thermal Expansion Glass Ceramics, Springer Berlin Heidelberg, Berlin, Heidelberg, 1995: pp. 1–12. https://doi.org/10.1007/978-3-662-03083-7_1.
[53] A. Zandonà, E. Véron, G. Helsch, A. Canizarès, J. Deubener, M. Allix, C. Genevois, Crystallization Mechanism of Gel-Derived SiO2–TiO2 Amorphous Nanobeads Elucidated by High-Temperature In Situ Experiments, Crystal Growth & Design. 23 (2023) 4545–4555. https://doi.org/10.1021/acs.cgd.3c00300.
[54] P. Fielitz, G. Helsch, G. Borchardt, J. Deubener, Al-26 and O-18 tracer diffusion in a titania-coated sodium aluminosilicate glass, Journal of Non-Crystalline Solids. 614 (2023) 122400. https://doi.org/10.1016/j.jnoncrysol.2023.122400.

[55] L. Cormier, Nucleation in Glasses – New Experimental Findings and Recent Theories, Procedia Materials Science. 7 (2014) 60–71. https://doi.org/10.1016/j.mspro.2014.10.009.
[56] A. Zandona, A. Martínez Arias, M. Gutbrod, G. Helsch, A.P. Weber, J. Deubener, Spray-Dried TiO2(B)-Containing Photocatalytic Glass-Ceramic Nanobeads, Advanced Functional Materials. 31 (2021) 2007760. https://doi.org/10.1002/adfm.202007760.
[57] W. Ostwald, Studien über die Bildung und Umwandlung fester Körper: 1. Abhandlung: Übersättigung und Überkaltung, Zeitschrift Für Physikalische Chemie. 22U (1897) 289–330. https://doi.org/doi:10.1515/zpch-1897-2233.
[58] A. Zandona, G. Helsch, J. Deubener, Inversion of quartz solid solutions at cryogenic temperatures, Journal of the American Ceramic Society. 103 (2020) 6630–6638. https://doi.org/10.1111/jace.17393.
[59] E. Kleebusch, C. Rüssel, C. Patzig, T. Höche, Evidence of epitaxial growth of high-quartz solid solution on ZrTiO4 nuclei in a Li2O-Al2O3-SiO2 glass, Journal of Alloys and Compounds. 748 (2018) 73–79. https://doi.org/10.1016/j.jallcom.2018.03.128.
[60] R. Roy, D.M. Roy, E.F. Osborn, Compositional and Stability Relationships Among the Lithium Aluminosilicates: Eucryptite, Spodumene, and Petalite, Journal of the American Ceramic Society. 33 (1950) 152–159. https://doi.org/10.1111/j.1151-2916.1950.tb12780.x.
[61] O. Dargaud, L. Cormier, N. Menguy, G. Patriarche, G. Calas, Mesoscopic scale description of nucleation processes in glasses, Appl. Phys. Lett. 99 (2011) 021904. https://doi.org/10.1063/1.3610557.
[62] Q. Zheng, J.C. Mauro, A.J. Ellison, M. Potuzak, Y. Yue, Universality of the high-temperature viscosity limit of silicate liquids, Phys. Rev. B. 83 (2011) 212202. https://doi.org/10.1103/PhysRevB.83.212202.
[63] D. Langhammer, D. Di Genova, G. Steinle-Neumann, Modeling the Viscosity of Anhydrous and Hydrous Volcanic Melts, Geochemistry, Geophysics, Geosystems. 22 (2021) e2021GC009918. https://doi.org/10.1029/2021GC009918.
[64] A.-M. Lejeune, P. Richet, Rheology of crystal-bearing silicate melts: An experimental study at high viscosities, Journal of Geophysical Research: Solid Earth. 100 (1995) 4215–4229. https://doi.org/10.1029/94JB02985.